Author Manuscript

Author Manuscript

Author Manuscript

Author Manuscript

HHS Public Access

Author manuscript

Ann Neurol. Author manuscript; available in PMC 2021 April 01.

Published in final edited form as:

Ann Neurol. 2020 April ; 87(4): 568–583. doi:10.1002/ana.25685.

Novel Recessive *TNNT1* Congenital Core-Rod Myopathy in French Canadians

David Pellerin, MD, MSc[1], **Asli Aykanat, MD**[2], **Benjamin Ellezam, MD, PhD**[3], **Emily C. Troiano, MS**[2], **Jason Karamchandani, MD**[4], **Marie-Josée Dicaire, BSc**[1], **Marc Petitclerc, MD**[5], **Rebecca Robertson, BSc**[1], **Xavier Allard-Chamard, MSc**[1], **Denis Brunet, MD**[6], **Chamindra G. Konersman, MD**[7], **Jean Mathieu, MD, MSc**[8,9], **Jodi Warman Chardon, MD, MSc**[10], **Vandana A. Gupta, PhD**[11], **Alan H. Beggs, PhD**[#2], **Bernard Brais, MDCM, MPhil, PhD**[#1,9,12], **Nicolas Chrestian, MD**[13]

[1]Department of Neurology and Neurosurgery, Montreal Neurological Hospital and Institute, McGill University, Montreal, Quebec, Canada;

[2]Division of Genetics and Genomics, The Manton Center for Orphan Disease Research, Boston Children's Hospital, Harvard Medical School, Boston, MA;

[3]Department of Pathology, Centre Hospitalier Universitaire Sainte-Justine, Université de Montréal, Montreal, Quebec, Canada;

[4]Department of Pathology, Montreal Neurological Hospital and Institute, McGill University, Montreal, Quebec, Canada;

[5]Department of Neurology, Hôpital Hôtel-Dieu de Lévis, Lévis, Quebec, Canada;

[6]Department of Neurology, Hôpital de l'Enfant Jésus, Université Laval, Quebec City, Quebec, Canada;

[7]Department of Neurosciences, University of California, San Diego, San Diego, CA;

[8]Faculty of Medicine and Health Sciences, Université de Sherbrooke, Sherbrooke, Quebec, Canada;

[9]Neuromuscular Disease Clinic, Centre Intégré Universitaire de Santé et de Services Sociaux du Saguenay-Lac-Saint-Jean, Jonquière, Quebec, Canada;

[10]Department of Neurosciences, Ottawa Hospital Research Institute, Ottawa, Ontario, Canada;

[11]Division of Genetics, Department of Medicine, Brigham and Women's Hospital, Harvard Medical School, Boston, MA;

[12]Department of Human Genetics, McGill University, Montreal, Quebec, Canada;

Address correspondence to Dr. Nicolas Chrestian, Centre Hospitalier de l'Université Laval et Centre Mère-Enfant Soleil, 2705 boulevard Laurier, Québec, QC, G1V 4G2, Canada. nicolas.chrestian.1@ulaval.ca.

Author Contributions

D.P., A.A., B.E., E.C.T., M-J.D., C.G.K., V.A.G, A.H.B., B.B., and N.C. contributed to the conception and design of the study; all authors contributed to acquisition and analysis of data; D.P., A.A., B.E., V.A.G, A.H.B., B.B., and N.C. contributed to drafting the manuscript and preparing the figures.

Potential Conflicts of Interest

Nothing to report.

Author Manuscript Author Manuscript Author Manuscript Author Manuscript

[13]Department of Child Neurology, Centre Hospitalier de l'Université Laval et Centre Mère-Enfant Soleil, Université Laval, Quebec City, Quebec, Canada

[#] These authors contributed equally to this work.

Abstract

Objective: Recessive null variants of the slow skeletal muscle troponin T1 (*TNNT1*) gene are a rare cause of nemaline myopathy that is fatal in infancy due to respiratory insufficiency. Muscle biopsy shows rods and fiber type disproportion. We report on 4 French Canadians with a novel form of recessive congenital *TNNT1* core-rod myopathy.

Methods: Patients underwent full clinical characterization, lower limb magnetic resonance imaging (MRI), muscle biopsy, and genetic testing. A zebrafish loss-of-function model using morpholinos was created to assess the pathogenicity of the identified variant. Wild-type or mutated human *TNNT1* mRNAs were coinjected with morpholinos to assess their abilities to rescue the morphant phenotype.

Results: Three adults and 1 child shared a novel missense homozygous variant in the *TNNT1* gene (NM_003283.6: c.287T > C; p.Leu96Pro). They developed from childhood very slowly progressive limb-girdle weakness with rigid spine and disabling contractures. They suffered from restrictive lung disease requiring noninvasive mechanical ventilation in 3 patients, as well as recurrent episodes of rhabdomyolysis triggered by infections, which were relieved by dantrolene in 1 patient. Older patients remained ambulatory into their 60s. MRI of the leg muscles showed fibrofatty infiltration predominating in the posterior thigh and the deep posterior leg compartments. Muscle biopsies showed multiminicores and lobulated fibers, rods in half the patients, and no fiber type disproportion. Wild-type *TNNT1* mRNA rescued the zebrafish morphants, but mutant transcripts failed to do so.

Interpretation: This study expands the phenotypic spectrum of *TNNT1* myopathy and provides functional evidence for the pathogenicity of the newly identified missense mutation.

The nemaline myopathies (NMs) are a group of genetically and clinically heterogeneous myopathies defined by the presence of nemaline rod inclusions in skeletal muscle fibers.[1] The phenotypic spectrum ranges from severe congenital forms to milder adult onset presentations.[2] Mutations in 13 genes encoding or regulating components of the sarcomeric thin filament complex are known to cause NMs.[3] Rare homozygous[4–9] and heterozygous[10] mutations in the slow skeletal muscle troponin T *(TNNT1)* gene have been linked to NM (nemaline myopathy 5, Amish type; MIM#605355). The recessive phenotype was first described in the Old Order Amish settlements of Pennsylvania, and presents with neonatal tremors and axial hypotonia, followed by progressive joint contractures, weakness, pectus carinatum, and restrictive lung disease.[4] Death from respiratory insufficiency ensues by the second year of life.[11] Six additional recessive *TNNT1* mutations were subsequently identified in non-Amish populations.[5–9] More recently, a dominant *TNNT1* missense variant was reported to cause a milder and heterogeneous phenotype.[10]

Herein, we report 4 individuals belonging to 3 apparently unrelated families of French Canadian ancestry harboring a novel homozygous *TNNT1* (NM_003283.6: c.287T>C;

Author Manuscript Author Manuscript Author Manuscript Author Manuscript

p.Leu96Pro) missense mutation causing a rare form of recessive congenital core-rod myopathy.

Subjects and Methods

Human Subjects

All subjects (Table) underwent serial clinical evaluations. Serum creatine kinase (CK), electrocardiogram, echocardiogram, and pulmonary function tests were obtained in all patients. Patients I, II, and III underwent electromyography. Magnetic resonance imaging (MRI) of the lower extremities and of the paraspinal muscles was acquired from Patients I, II, and III, and from Patients II and III, respectively. The institutional review board (IRB) of the Centre Hospitalier Universitaire de Montréal approved this study (ND02.046), and all patients or their legal guardians provided written informed consent. Control muscle biopsies were obtained from 3 females and 1 male under an IRB-approved protocol through the Clinical Biological Research and Genetic Repository of the Montreal Neurological Institute (15–944-MUHC).

Muscle Pathology

Open muscle biopsies were obtained from quadriceps (Patients I, II, III, and IV) and deltoid (Patient III). Standard techniques were used for histochemical, immunohistochemical, and histoenzymological staining. Electron microscopy was performed on muscle specimens fixed fresh with glutaraldehyde.

Genetic Sequencing

Next generation sequencing was performed using a comprehensive myopathy gene panel (Supplementary Table). For segregation analysis, the candidate variant in the *TNNT1* gene was Sanger sequenced in selected first-degree relatives following written informed consent.

Fish and Embryo Maintenance

Zebrafish *(Danio rerio)* were maintained as previously described.[12] AB or Casper fish were used for all experiments. Animal work was performed with approval from the Boston Children's Hospital institutional animal care and use committee (17-05-3454R). All studies were conducted in accordance with the US Public Health Service's Policy on Humane Care and Use of Laboratory Animals.

Morpholino Knockdown and mRNA Rescue

Two antisense morpholinos (MOs; Gene Tools, Philomath, OR), 1 targeting the translational ATG site *(tnnt1* TR-MO) and 1 targeting the splice acceptor site between intron 7 and exon 8 *(tnnt1* SP8-MO), were designed to knock down the zebrafish *tnnt1* gene (Ensembl-ID: ENSDARG00000037954). The MO sequences were *tnnt1* TR-MO: 5'-ATTCCTCTTCTACATCA GACATGAT-3' and *tnnt1* SP8-MO: 5'-CCTGTAATGTGGAG GACAAAAGCAA-3'. MOs were dissolved in ×1 Danieau buffer with 0.1% phenol red. Five nanograms of *tnnt1* TR-MO and 1ng of *tnnt1*SP8-MO were injected into the fertilized yolks of 1-cell embryos.

Author Manuscript Author Manuscript Author Manuscript Author Manuscript

For rescue experiments, full-length *Homo sapiens TNNT1* (NM_003283.6) cDNA was cloned into a pCS2^{+} vector (from Dr Nathan D. Lawson, Addgene plasmid #22423) using Gateway technology (Invitrogen, Carlsbad, CA). The *TNNT1* c.287T>C (p.Leu96Pro) substitution was introduced using the Q5 Site-Directed Mutagenesis Kit (Invitrogen). The mRNAs for both wild-type (WT) and c.287T>C mutant constructs were synthesized in vitro using mMessenger Kit (Ambion, Austin, TX) and purified using mini Quick Spin RNA columns (Roche, Basel, Switzerland). One hundred picograms of mRNA was injected into randomly selected 1-cell stage embryos.

Phenotyping and Birefringence

Fertilized 1-cell zebrafish embryos were injected with MOs and mRNAs and were staged by days postfertilization (dpf). Embryos were counted at 1 dpf and 3 dpf. Three-dpf embryos were phenotyped, and muscle birefringence was analyzed as previously described.[13] Representative images were taken under similar conditions with 50 milliseconds of exposure using a Carl Zeiss (Oberkochen, Germany) Discovery V8 Stereo microscope.

Reverse Transcription and Quantitative Polymerase Chain Reaction

RNA was extracted from human muscle biopsies using TRIzol reagent. cDNA was synthesized from DNase-treated RNA using the SuperScript III Kit (Thermo Fisher Scientific, Waltham, MA). Polymerase chain reaction (PCR) was performed with Taq polymerase (Qiagen, Valencia, CA) using primers for *TNNT1* exons 7 to 9 (forward: GTGGTGCCTCCTTTGATCC; reverse: CTTGGCCTCTTCCTCTTCCT), exon 5 (forward: GGCTC GCCTCAAGATTCAC; reverse: TCCAGCAGGTCTTTCTCC AT), and exon 12 (forward: GCAGAACAGAAGCGTGGTAA; reverse: GCCATCAGGTCGAACTTCTC). PCR products were resolved on a 3% agarose gel containing ethidium bromide.

For zebrafish knockdowns, embryos were injected with 1.0 or 2.5ng of *tnnt1* SP8-MO, and 10 embryos per condition were collected at 7 dpf. RNA was extracted using RNeasy Fibrous Tissue Mini Kit (Qiagen), and cDNA was synthesized using the SuperScript IV Kit (Thermo Fisher Scientific). cDNA was amplified by reverse transcription (RT)-PCR, using primers flanking exons 6 and 9 of *tnnt1* (forward: CAGAGGAAGCTGGAACAGAAC; reverse: CGCCGCTCAATTCTATCCTTTA). EF1a was used as control. RT-PCR products were isolated by gel extraction using QIAquick Gel Extraction Kit (Qiagen) or TOPO TA Cloning Kit (Thermo Fisher Scientific). Resulting products were Sanger sequenced.

For quantitative RT-PCR experiments, cDNA was synthesized from DNase-treated RNA with the High Capacity cDNA Reverse Transcription Kit (Applied Biosystems, Foster City, CA). Quantitative PCR was performed on a QuantStudio 7 Flex Real-Time PCR System (Applied Biosystems) using the TaqMan Fast Advanced assay (Applied Biosystems). For each gene assay, samples were run in duplicate and *TNNT1* levels were normalized against expression of *TBP* The following assays were used: *TNNT1* (NM_003283.6, NM_001126132.2, NM_001126133.2, NM_00129177.1) and *TBP* (NM_003194.3). Relative quantification was computed by the $2^{-\Delta\Delta Ct}$ method using the mean value of controls as calibrator. Data were analyzed with the QuantStudio Software v1.3 (Applied Biosystems).

Author Manuscript Author Manuscript Author Manuscript Author Manuscript

Immunoblotting

Muscle tissues were homogenized in RIPA lysis buffer supplemented with protease inhibitor cocktail. After sonication and centrifugation, protein samples were mixed with Laemmli buffer containing dithiothreitol and heated at 70°C for 10 minutes. Protein extracts were resolved by sodium dodecyl sulfate–polyacrylamide gel electrophoresis (4–12%) and transferred onto nitrocellulose membrane. After blocking in 5% nonfat dry milk and 3% bovine serum albumin in 0.1% Tween-20/Tris-buffered saline (TBS), the membrane was incubated with mouse monoclonal antibody anti–troponin T (clone CT3; Santa Cruz Biotechnology, Santa Cruz, CA; sc-20025, 1:500) or muscle-specific anti–sarcomeric alpha-actinin (clone EA-53; Abcam, Cambridge, MA; ab66186, 1:2,500). The membrane was then incubated with horseradish peroxidase–conjugated goat antimouse IgG antibody (Jackson ImmunoResearch, West Grove, PA; 1:10,000). Western blots were developed using enhanced chemiluminescent reagent.

For zebrafish knockdowns, the Casper line was used to generate *tnnt1* SP8-MO knockdowns. At 3 dpf, the uninjected control embryos and the MO knockdowns were phenotyped and 40 embryos were selected from each condition twice. Euthanized zebrafish embryos were homogenized with M-PER extraction reagent (Pierce, Rockford, IL) supplemented by proteinase K inhibitor. Immunoblotting was performed as described above with anti–troponin T antibody (clone CT3, 1:500) or with mouse monoclonal anti-vinculin antibody (clone VIN-11–5; Sigma, St Louis, MO; V4505, 1:1,000).

Immunofluorescence

After fixation in 4% paraformaldehyde, muscle sections were permeabilized (5% donkey serum, 0.1% Triton X-100, and 1% glycine in TBS) for 1 hour at room temperature then incubated with anti–troponin T antibody (clone CT3, 1:100) overnight at 4°C. The sections were subsequently washed in TBS and incubated with anti-mouse Alexa Fluor 555 (Abcam, ab150106, 1:500) and Alexa Fluor 647 phalloidin (Invitrogen, A22287, 1:40). Slides were mounted with ProLong Gold reagent with DAPI (Invitrogen). Images were acquired with a Leica Microsystems (Wetzlar, Germany) TCS-SP8 confocal microscope.

Zebrafish embryos at 3 dpf were anesthetized with 4% tricaine and fixed using 4% paraformaldehyde overnight at room temperature. Embryos were washed in phosphate-buffered saline, 0.1% Tween, and 2% Triton and blocked with 5% goat serum. Phalloidin (Alexa Fluor 488, Invitrogen, A12379) and Hoechst-33342 (Life Technologies, Carlsbad, CA) were used for staining. Fish were mounted with 3% methylcellulose, and representative images were taken by a spinning disc confocal microscope.

Electron Microscopy and Toluidine Blue Staining

Three dpf embryos were fixed in 2.5% paraformaldehyde, 5.0% glutaraldehyde, 0.06% picric acid in 0.2M cacodylate buffer overnight at 4°C. Samples were then embedded, cut into 50nm-thin sections, and stained with toluidine blue. Representative pictures were taken using a Nikon (Tokyo, Japan) Eclipse 50i, and the electron microscopy images were viewed with a JEOL (Tokyo, Japan) 1200EX–80kV.

Author Manuscript Author Manuscript Author Manuscript Author Manuscript

Results

Phenotype Analysis

A summary is provided in the Table. All subjects were French Canadian and born from nonconsanguineous parents, except for Patient IV, whose parents were third-degree cousins. Patients I and II were a 62-year-old female and her 53-year-old brother. They had 7 healthy siblings. Patient III was an 8-year-old female only child, and Patient IV was a 46-year-old female. Her younger sister was healthy.

At birth, Patient III was found to have arthrogryposis multiplex congenita, congenital scoliosis, and rigid spine. Although the contractures improved over the following years, she was left with elbow and hip contractures (Fig 1). The neonatal period was otherwise unremarkable for the other subjects. None had neonatal tremor or axial hypotonia. Delays in gross motor milestones were evident in all patients from infancy. Independent walking was achieved at a median of 30 months of age (range = 14–36 months). All patients developed since infancy very slowly progressive proximal muscle weakness, affecting the shoulder and hip girdles except in Patient IV, in whom weakness was restricted to the hip girdle, neck flexors, and tibialis anterior muscles. Relentlessly progressive joint contractures severely limited shoulder, elbow, wrist, finger, hip, and ankle range of motion in Patients I and II. Patient IV suffered from progressive hip and ankle contractures, whereas Patient III had static flexion contractures of the hips and elbows. All patients displayed spinal rigidity, scoliosis, short stature, myopathic facies, and high-arched palate. They showed no bulbar weakness, scapular winging, or pectus carinatum. Restrictive pulmonary syndrome was mild in Patient I, moderate in Patient II, and severe in Patients III and IV. Patient IV required bilevel positive airway pressure (BiPAP) ventilation throughout the day and night. Patients II and III also suffered from obstructive sleep apnea, for which they used BiPAP at night. The age of initiation of noninvasive ventilation was 53, 4, and 36 years for Patients II, III, and IV, respectively. Upright and supine spirometry in Patients I, II, and III did not reveal preferential diaphragmatic involvement. All subjects experienced few to several episodes of painful rhabdomyolysis following febrile illness or surgery. All patients complained of muscle cramps during or after physical activity. Baseline CK ranged from normal to 4 times higher than normal. Prophylactic treatment with dantrolene (1mg/kg every 6 hours for 2 days) in Patient III given at time of infection or surgery either prevented or alleviated rhabdomyolysis. None of the 3 adult subjects has yet been given dantrolene. All subjects remain variably ambulatory. Patients I and II walk unaided. Both were never able to run or use stairs without support. Although Patient III acquired walking at 36 months of age, she can now walk long distances and climb a few stairs unaided. Patient IV began using a wheelchair at age 14 years as a consequence of worsening muscle weakness and respiratory function. She is able to walk 20 steps with assistance. Electrocardiogram and echocardiogram were normal. Electromyogram in Patients I and II showed mild myopathic potentials in the former and normal potentials in the latter. Patient III had normal electromyographic evaluation at age 1 year.

Author Manuscript Author Manuscript Author Manuscript Author Manuscript

Muscle MRI Findings

Muscle MRIs of the lower extremities were performed in Patient I at age 57 years and Patient II at age 53 years and revealed marked atrophy and fatty infiltration of the posterior thigh compartment, in particular of the semimembranosus, and adductor muscles, with sparing of the gracilis muscles. Myopathic changes were observed in the distal leg muscle groups, predominating in the tibialis anterior, soleus, and deep posterior leg compartment (Fig 2). The gastrocnemius muscles were spared. MRI findings were symmetrical and followed a proximal-to-distal severity gradient. Patient III underwent a muscle MRI of the lower extremities at age 6 years. Of note, the MRI scan was performed 1 week following an episode of rhabdomyolysis, which likely accounted for an asymmetric hyperintense T2 signal suggestive of myoedema in several muscle groups. Myopathic changes were found in the semimembranosus and the adductor group, with the exclusion of the gracilis muscle, but not in the deep posterior leg compartment. Paraspinal muscle MRI revealed diffuse atrophy and fatty infiltration in Patients II and III.

Muscle Pathology

Biopsies of the quadriceps were obtained from all patients at age 59 (Patient I), 48 (Patient II), 8 (Patient III), and 9 years (Patient IV). Patient III had also undergone a deltoid biopsy at age 5 years. The main histopathological findings are summarized in the Table, and representative images taken from Patients I and III are shown in Figure 3. All muscle biopsies showed multiple, small, irregular defects on nicotinamide adenine dinucleotide dehydrogenase–tetrazolium reductase consistent with multiminicores, in the vast majority of type I fibers. Approximately 30 to 40% of affected fibers appeared lobulated, due to the pattern of mitochondrial accumulation, as evidenced on electron microscopy. Electron microscopy confirmed the presence of multiminicores in the form of small irregular areas of myofibrillar disorganization excluding mitochondria. Patients I and II showed nemaline rods in 30 to 40% of type I fibers, in the same fibers that were lobulated and showed minicores. Although some isolated rods were located in the intermyofibrillar space, most of them clustered to form large globular subsarcolemmal inclusions. These findings were exclusive to type I fibers. Triads' morphology and organization appeared normal in Patient I's biopsy. All biopsies showed moderate variation in fiber size and shape, with most of the variability occurring in type I fibers. None of the biopsies showed fiber type disproportion, but selective type II fiber atrophy was present in 1 biopsy (Patient II). All biopsies showed very focal endomysial fibrosis and fatty infiltration, and 1 biopsy (Patient III, quadriceps) had scattered regenerative fibers.

Genetic Diagnosis

Next generation sequencing identified a novel homozygous missense variant in the *TNNT1* gene (NM_003283.6: c.287T>C; p.Leu96Pro) in all patients. No pathogenic variants were found in other genes known to cause congenital NMs, core myopathy, or myopathy associated with joint and/or spinal contractures. This variant was predicted to be pathogenic by different bioinformatic software.[14–16] Combined Annotation Dependent Depletion predicted a scaled PHRED score of 26.6.[17] The leucine residue at position 96 is located in exon 8 of the *TNNT1* gene and is highly conserved.[18] Leucine to proline substitution is

Author Manuscript Author Manuscript Author Manuscript Author Manuscript

predicted to result in disruption of the alpha-helical secondary structure at the tropomyosin-binding site 1,[16] encoded by *TNNT1* exons 7 through 9.[19] Moreover, the frequency of the *TNNT1* c.287T>C allele is very low (3.98e-6) in the Genome Aggregation Database,[20] with no previous report of homozygosity. This variant was absent from ClinVar[21] and the Human Gene Mutation Databse.[22] Targeted sequencing of *TNNT1* in each family supported segregation of the homozygous *TNNT1* missense variant with disease in our patients (see Fig 1I–K).

Molecular Characterization of *TNNT1*

To investigate the molecular consequences of the c.287T>C variant, we assessed *TNNT1* expression at the mRNA and protein levels in patients' muscle (Fig 4). Quantitative RT-PCR did not show a significant difference in levels of *TNNT1* transcripts in skeletal muscle between patients and controls. The *TNNT1* gene contains 14 exons, and alternative splicing of exon 5 generates high and low molecular weight slow skeletal muscle troponin T (TnTs) splice forms, respectively known as isoform 1 and isoform 2.[19] Normal slow skeletal muscle mainly expresses the high molecular weight TnTs isoform.[23] A longer exon 12 (exon 12') resulting from partial retention of intron 11 also arises from alternative splicing.[10,24] The low molecular weight TnTs produced from transcripts lacking exon 5 was previously shown to generate more contractile force[23,24] and to be upregulated in patients with dominantly inherited *TNNT1* NM as a physiological adapta-tion.[10] We sought to establish whether these findings were recapitulated in patients homozygous for the *TNNT1* c.287T>C mutation using RT-PCR. We did not observe increased relative expression of *TNNT1* transcripts lacking exon 5 in patients compared to controls. Specifically, the low molecular weight splice form was expressed at 29.8% of total *TNNT1* transcripts in patients as compared to 28.1% in controls. The exon 12' was not expressed in any patient or control muscle.

Muscle expression of TnTs was next analyzed by immunoblotting. This demonstrated a marked reduction close to 75% in the levels of the high molecular weight TnTs isoform in patients relative to controls. In comparison, levels of the low molecular weight isoform were not significantly different in patient and control muscle. Semi-quantitative analysis of the immunoblots revealed that the small isoform of TnTs represented 44.6 ± 7.8% of total TnTs in patients, whereas this ratio was only 19.8 ± 4.2% in controls ($p = 0.003$, Student t test). We next aimed to ascertain by immunofluorescence whether the subcellular localization of the mutant protein was altered. Mislocalization of TnTs in relation to F-actin was not appreciated in patients compared to controls.

Zebra fish Model of Recessive *TNNT1* Myopathy

The zebrafish genome includes a single orthologue of human *TNNT1*, designated *tnnt1*, on chromosome 3.[25] The canonical *tnnt1*-201 transcript (NM_001128695.1) encodes a 268–amino-acid protein that has 70% identity and 82% similarity with human TnTs isoform a (NP_003274.3) and 75% and 89% identity and similarity, respectively, with human isoforms b and c (NP_001119604.1, NP_001119605.1). To knockdown the *tnnt1* gene in zebrafish, 2 MOs were designed to target the translational ATG site (*tnnt1* TR-MO) and the splice acceptor site of exon 8 (*tnnt1* SP8-MO). Each MO was injected into 1-cell stage embryos, and resulting fry were phenotyped at 3 dpf. Both MOs induced similar myopathic

Author Manuscript Author Manuscript Author Manuscript Author Manuscript

phenotypes characterized by reduced muscle mass and variable degrees of dorsal curvature (Fig 5A). To verify the mechanism of action of *tnnt1* SP8-MO, RT-PCR was performed on 7 dpf morphants. Although the RT-PCR revealed a decreased amount of WT *tnnt1* transcript with increasing doses of SP8-MO injections, sequencing of the RT-PCR products showed 3 additional transcripts where exons 7 and 8 were spliced out, exon 8 was spliced out, or the intron between exons 7 and 8 was retained (Fig 6A, B). Furthermore, immunoblotting showed decreased level of TnTs expression in morphants compared to WT larvae (see Fig 6C). The *tnnt1* SP8-MO morphants demonstrated mild to severe truncal curvature along with reduced birefringence in contrast to uninjected control WT larvae, which displayed straight morphology without loss of birefringence. Immunofluorescence revealed disorganized and reduced numbers of myofibers spaced farther away from each other in *tnnt1* SP8-MO morphants compared to WT controls (see Fig 5B). Electron microscopy of cross sections showed disorganized sarcomeres and Z-line thickening in both slow and some fast myofibers of *tnnt1* SP8-MO morphants at 3 dpf (Fig 7A–C). The zebrafish *tnnt1* gene appears to be under slightly relaxed transcriptional control relative to other slow muscle specific genes,[26] and persistence of defects at 3 to 7 dpf may reflect the consequences of gene knockdown in early uncommitted muscle precursor cells. Examination of longitudinal skeletal muscle sections in *tnnt1* SP8-MO morphants (3 dpf) also revealed corelike intramyofibrillar areas of sarcomeric disorganization, which together with Z-line thickening (see Fig 7D–F) are reminiscent of the ultra-structural changes seen in human patients.

To confirm the specificity of action of the *tnnt1* MOs, morphants were coinjected with full-length WT human *TNNT1* mRNA. Both the altered body shape and reduced birefringence were corrected in SP8-MO morphants (see Fig 5A, C, D), supporting the functional equivalence of TnTs with the zebrafish *tnnt1* gene product, and demonstrating that the morphant phenotype is largely due to action of the MO on *tnnt1* mRNAs.

We next evaluated the impact of the *TNNT1* c.287T>C variant on the ability of injected mRNA to rescue the morphological abnormalities of *tnnt1* SP8-MO morphants. In contrast to the rescue experiments using WT human *TNNT1* mRNA, coinjecting the mutated human mRNA with *tnnt1* SP8-MOs failed to rescue the truncal curvature (see Fig 5C), although immunoblotting confirmed increased levels of TnTs in fish injected with either the WT or c.287T>C transcripts (data not shown). Similarly, the mutated mRNA was unable to rescue the birefringence phenotype of the *tnnt1* SP8-MO morphants in comparison to WT *TNNT1* mRNA (see Fig 5D), suggesting that the mutational mechanism of p.Leu96Pro involves a loss of function. Injection of *TNNT1* c.287T>C mRNA alone into WT embryos had no deleterious effects (data not shown), consistent with the recessive nature of this mutation.

Discussion

This study describes the first pathogenic homozygous *TNNT1* missense variant (NM_003283.6: c.287T>C; p.Leu96Pro). The *TNNT1* gene encodes the tropomyosin-binding troponin T isoform TnTs, expressed in type I skeletal myofibers. TnTs anchors the troponin complex onto the thin filament through its 2 tropomyosin-binding domains. These 2 domains are encoded by *TNNT1* exons 7 through 9 and exon 11, respectively.[19] All previously reported pathogenic recessive *TNNT1* variants were null or loss-of-function

Author Manuscript Author Manuscript Author Manuscript Author Manuscript

mutations resulting from exonic loss[4–9] that rendered the TnTs subunit unable to form the troponin complex or to incorporate into thin filaments and, as a result, led to degradation of the truncated protein.[19,27–29] In comparison, the *TNNT1* c.287T>C mutation in exon 8 shared by our patients substitutes the highly conserved[18] leucine residue at position 96 with proline, and results in disruption of the alpha-helical secondary structure of the tropomyosin-binding site 1.[16] This is predicted to have a deleterious effect on the binding affinity of TnTs for tropomyosin. The misattached mutant TnTs is likely to inefficiently incorporate into myofilaments and to undergo partial decay as suggested by the substantially lower levels of total TnTs detected in our patients' muscle. This phenomenon likely spares the low molecular weight TnTs, because this isoform has a higher binding affinity for tropomyosin.[23,27] The remaining nondegraded TnTs likely maintains a functional interaction, albeit weakened, with tropomyosin. The preferential retention of the low molecular weight isoform, which generates more contractile force than the high molecular weight variant,[23,24] and the incomplete degradation of TnTs likely account for the milder phenotype of our subjects compared to patients with *TNNT1*-null myopathy.

Clinically, our patients exhibited a rather homogeneous phenotype that was milder than that of the recessive *TNNT1*-null myopathy.[4–7] Certain core clinical features were reminiscent of the severe recessive phenotype, including the association of limb-girdle weakness with multiple contractures, rigid spine, and kyphoscoliosis. Our patients nonetheless lacked neonatal hypotonia and tremors as well as pectus carinatum.[4,11] Despite proximal weakness, most retained independent ambulation, even up into their 60s for older patients. They also suffered from variable restrictive lung disease as a result of chest wall rigidity and kyphoscoliosis. Short stature was another consistent feature observed in our group of patients, which may reflect a limited growth potential resulting from the additive effect of muscle weakness, joint contractures, and rigid spine.

A combination of structural changes in muscle cytoarchitecture and extrinsic mechanical factors likely contributed to development of contractures in our cohort. A mild degree of fibrofatty infiltration of muscle fibers was shown on muscle MRI and biopsies of our patients, and such change is known to result in reduced extensibility and chronic shortening of muscles.[30,31] The disruption of normal sarcomeric architecture and myofibrillar organization are additional changes implicated in formation of contractures through adaptive compensatory shortening of muscles.[32] These pathological changes may reflect an ongoing myofibrillar breakdown process caused by failure of the excitation–contraction coupling mechanism. How this myofibrillar disruption might lead to elevated baseline CK levels is unclear, but the histological evidence for increased endomysial fibrosis, particularly in older patients, suggests an ongoing myopathic process involving some degree of dystrophic progression. Interestingly, regenerative activity was lacking or at most mild in muscle biopsies, suggesting a weakened proliferative potential of the satellite cells as previously described in NMs.[33]

The occurrence of recurrent episodes of rhabdomyolysis triggered by febrile illness is one of the most salient features of the French Canadian *TNNT1* myopathy. To our knowledge, this is the first description of a *TNNT1* mutation provoking rhabdomyolysis. Baseline CK levels were also found to be up to 4 times higher than normal between the episodes. This is in

Author Manuscript Author Manuscript Author Manuscript Author Manuscript

contrast to the normal CK levels in previously reported cases of *TNNT1* myopathy.[10,11] The use of the sarcoplasmic reticulum ryanodine receptor blocker dantrolene to prevent rhabdomyolysis in 1 patient may suggest hypersensitivity of the mutated troponin complex to calcium.

The slow skeletal muscle isoform and the cardiac isoform of troponin T are highly homologous proteins.[34] The cardiac isoform of troponin T (TnTc) is found at low levels in normal adult skeletal type I myofibers, consistent with its homology with TnTs.[19,35,36] Missense variants in the alpha-helical tropomyosin-binding domain of TnTc decrease its binding affinity for tropomyosin while rendering the thin filament complex hypersensitized to calcium.[37,38] The hypersensitized state arises as a consequence of a slower rate of calcium dissociation from the mutated troponin complex.[38] A similar mechanism may be implicated in the pathogenesis of rhabdomyolysis in our patients. Furthermore, a recent study showed a compensatory upregulation of TnTc in spindle intrafusal myofibers of TnTs-knockout mice.[39] This change results in an abnormally high sensitivity of spindle fibers for calcium, as TnTc possesses a stronger affinity for calcium than TnTs.[39] Although the intrafusal TnT isoform composition was not established in our patients, it is possible that they also upregulate TnTc. Interestingly, low molecular weight TnT isoforms were previously shown to possess lower calcium sensitivity.[40,41] The preferential expression of the low molecular weight TnTs splice form in our patients' muscle may therefore play a role in dampening the heightened myofilament sensitivity to calcium. It would be interesting to confirm this hypothesis by examining calcium dynamics in relation to excitation–contraction coupling in the muscle of patients with the p. Leu96Pro *TNNT1* myopathy.

Typical histological features of *TNNT1* NM include rods in type I and II fibers, increased fiber size variation, fiber type disproportion, and selective type II fiber hypertrophy.[5–7,10,11] Except for mild to moderate fiber size variation, these findings were lacking in our cases. Nemaline rods were found in about 30 to 40% of type I fibers in half the patients. The most distinctive structural abnormality observed in all patients was the presence of multiminicores in the majority of type I fibers. This is the first report of core-rod pathology in *TNNT1*-related myopathy.[1]

As part of this study, we intended to utilize the zebrafish *tnnt1* morphant model to strengthen the evidence for pathogenicity of the *TNNT1* c.287T>C variant. The results of the rescue experiments, which showed that injection of human WT *TNNT1* mRNA but not *TNNT1* c.287T>C mRNA led to robust rescue of the zebrafish *tnnt1* morphant phenotype, provide strong evidence to support this conclusion. Although WT *TNNT1* mRNA failed to rescue a fraction of the morphants, the level of rescue we achieved is similar to that obtained in other comparable studies.[42–44] Furthermore, RNA-based rescue experiments are known to rarely result in complete rescue due to several technical factors such as different levels and expression of MOs and mRNAs in individual cells and limited stability of mRNAs during the first few days of development, which is a limitation of the transient expression systems.[45] MO-generated phenotypes tend to be more severe and less specific than those of the corresponding mutants; this is attributed to phenotypic rescue of zygotic mutants by maternally provided mRNA, which can be blocked by MOs or due to genetic compensation in the mutants.[46] The phenotype of our model is comparable to the severe phenotype

Author Manuscript Author Manuscript Author Manuscript Author Manuscript

observed in other morphant models of recessive congenital myopathies.[42,43,47–50] There is also a possibility of off-target effects of MOs; this was, however, ruled out, as we showed rescue of the morphant phenotype by the WT *TNNT1* mRNA but not the mutant *TNNT1* mRNA. Remarkably, corelike intramyofibrillar areas, sarcomeric disorganization, and Z-line thickening that are reminiscent of the changes seen in human patients were observed in the *tnnt1* morphants, suggesting specificity of our model for the human disease. In future studies, many limitations of the morphant model could be circumvented by the use of a CRISPR (clustered regularly interspaced short palindromic repeats)-engineered zebrafish mutant, which would allow for a more in-depth analysis of *tnnt1* biology in zebrafish.

In summary, we report 4 French Canadian patients with a unique form of recessive *TNNT1* congenital core-rod myopathy associated with episodic rhabdomyolysis caused by a functionally confirmed novel missense mutation. The milder phenotype and favorable prognosis expand the spectrum of recessive *TNNT1*-related myopathy.

Supplementary Material

Refer to Web version on PubMed Central for supplementary material.

Acknowledgment

This work was supported by grants G247655 from the Montreal General Hospital Foundation, R01HD075802 from the NIH National Institute of Child Health and Human Development, and MDA602235 from the Muscular Dystrophy Association (USA), and a generous gift from the Lee and Penny Anderson Family Foundation. Molecular genetic support services were provided by the Boston Children's Hospital Intellectual and Developmental Disabilities Research Center Molecular Genetics Core Facility supported by U54HD090255 from the NIH Eunice Kennedy Shriver National Institute of Child Health and Human Development. The funders had no role in the conduct of this study.

The *TNNT1*plasmid was provided by the ORFeome Collaboration (plasmid clone ID: HsCD00368188). Storage and distribution were provided by the PlasmID Repository at Harvard Medical School and by NIH National Cancer Institute cancer center support grant P30CA06516.

We thank the patients and their families for allowing us to publish this clinical report; and the Neuro Microscopy Imaging Center for assistance in imaging human specimens for this research. pCSDest was a gift from Dr. N. D. Lawson (Addgene plasmid #22423).

Additional supporting information can be found in the online version of this article.

References

1. Jungbluth H, Treves S, Zorzato F, et al. Congenital myopathies: disorders of excitation-contraction coupling and muscle contraction. Nat Rev Neurol 2018;14:151–167. [PubMed: 29391587]
2. Ryan MM, Schnell C, Strickland CD, et al. Nemaline myopathy: a clinical study of 143 cases. Ann Neurol 2001;50:312–320. [PubMed: 11558787]
3. Malfatti E, Romero NB. Nemaline myopathies: state of the art. Rev Neurol (Paris) 2016;172:614–619. [PubMed: 27659899]
4. Johnston JJ, Kelley RI, Crawford TO, et al. A novel nemaline myopathy in the Amish caused by a mutation in troponin T1. Am J Hum Genet 2000;67:814–821. [PubMed: 10952871]
5. Abdulhaq UN, Daana M, Dor T, et al. Nemaline body myopathy caused by a novel mutation in troponin T1 (TNNT1). Muscle Nerve 2016;53:564–569. [PubMed: 26296490]
6. Marra JD, Engelstad KE, Ankala A, et al. Identification of a novel nemaline myopathy-causing mutation in the troponin T1 (TNNT1) gene: a case outside of the old order Amish. Muscle Nerve 2015;51: 767–772. [PubMed: 25430424]

Author Manuscript Author Manuscript Author Manuscript Author Manuscript

7. van der Pol WL, Leijenaar JF, Spliet WG, et al. Nemaline myopathy caused by TNNT1 mutations in a Dutch pedigree. Mol Genet Geno-micMed 2014;2:134–137.
8. Fattahi Z, Kalhor Z, Fadaee M, et al. Improved diagnostic yield of neuromuscular disorders applying clinical exome sequencing in patients arising from a consanguineous population. Clin Genet 2017; 91:386–402. [PubMed: 27234031]
9. D'Amico A, Fattori F, Fiorillo C, et al. 'Amish nemaline myopathy' in 2 Italian siblings harbouring a novel homozygous mutation in troponin-I gene. Neuromuscul Disord 2019;29:766–770. [PubMed: 31604653]
10. Konersman CG, Freyermuth F, Winder TL, et al. Novel autosomal dominant TNNT1 mutation causing nemaline myopathy. Mol Genet Genomic Med 2017;5:678–691. [PubMed: 29178646]
11. Fox MD, Carson VJ, Feng HZ, et al. TNNT1 nemaline myopathy: natural history and therapeutic frontier. Hum Mol Genet 2018;27: 3272–3282. [PubMed: 29931346]
12. Westerfield M The zebrafish book. A guide for the laboratory use of zebrafish (Danio rerio). 5th ed Eugene, OR: University of Oregon Press, 2007.
13. Smith LL, Beggs AH, Gupta VA. Analysis of skeletal muscle defects in larval zebrafish by birefringence and touch-evoke escape response assays. J Vis Exp 2013;82:e50925.
14. Adzhubei IA, Schmidt S, Peshkin L, et al. A method and server for predicting damaging missense mutations. Nat Methods 2010;7: 248–249. [PubMed: 20354512]
15. Choi Y, Sims GE, Murphy S, et al. Predicting the functional effect of amino acid substitutions and indels. PLoS One 2012;7:e46688. [PubMed: 23056405]
16. Venselaar H, Te Beek TA, Kuipers RK, et al. Protein structure analysis of mutations causing inheritable diseases. An e-Science approach with life scientist friendly interfaces. BMC Bioinformatics 2010; 11:548. [PubMed: 21059217]
17. Rentzsch P, Witten D, Cooper GM, et al. CADD: predicting the deleteriousness of variants throughout the human genome. Nucleic acids Res 2019;47:D886–D894. [PubMed: 30371827]
18. Ashkenazy H, Erez E, Martz E, et al. ConSurf 2010: calculating evolutionary conservation in sequence and structure of proteins and nucleic acids. Nucleic Acids Res 2010;38(Web Server issue): W529–W533. [PubMed: 20478830]
19. Mondal A, Jin JP. Protein Structure-function relationship at work: learning from myopathy mutations of the slow skeletal muscle isoform of troponin T. Front Physiol 2016;7:449. [PubMed: 27790152]
20. Collins RL, Brand H, Karczewski KJ, et al. An open resource of structural variation for medical and population genetics. bioRxiv 2019; 578674:1–15.
21. Landrum MJ, Lee JM, Benson M, et al. ClinVar: improving access to variant interpretations and supporting evidence. Nucleic Acids Res 2018;46(D1):D1062–D1067. [PubMed: 29165669]
22. Stenson PD, Ball EV, Mort M, et al. Human Gene Mutation Database (HGMD): 2003 update. Human Mutat 2003;21:577–581.
23. Larsson L, Wang X, Yu F, et al. Adaptation by alternative RNA splicing of slow troponin T isoforms in type 1 but not type 2 Charcot-Marie-Tooth disease. Am J Physiol Cell Physiol 2008;295: C722–C731. [PubMed: 18579801]
24. Zhang T, Choi SJ, Wang ZM, et al. Human slow troponin T (TNNT1) pre-mRNA alternative splicing is an indicator of skeletal muscle response to resistance exercise in older adults. J Gerontol A Biol Sci Med Sci 2014;69:1437–1447. [PubMed: 24368775]
25. Ferrante MI, Kiff RM, Goulding DA, Stemple DL. Troponin T is essential for sarcomere assembly in zebrafish skeletal muscle. J Cell Sci 2011;124(pt 4):565–577. [PubMed: 21245197]
26. Jackson HE, Ono Y, Wang X, et al. The role of Sox6 in zebrafish muscle fiber type specification. Skelet Muscle 2015;5:2. [PubMed: 25671076]
27. Amarasinghe C, Hossain MM, Jin JP. Functional basis of three new recessive mutations of slow skeletal muscle troponin T found in non-AmishTNNT1 nemalinemyopathies. Biochemistry 2016;55:4560–4567. [PubMed: 27429059]
28. Wang X, Huang QQ, Breckenridge MT, et al. Cellular fate of truncated slow skeletal muscle troponin T produced by Glu180 nonsense mutation in Amish nemaline myopathy. J Biol Chem 2005;280: 13241–13249. [PubMed: 15665378]

Author Manuscript Author Manuscript Author Manuscript Author Manuscript

29. Jin JP, Brotto MA, Hossain MM, et al. Truncation by Glu180 nonsense mutation results in complete loss of slow skeletal muscle troponin T in a lethal nemaline myopathy. J Biol Chem 2003;278: 26159–26165. [PubMed: 12732643]
30. McDonald CM. Limb contractures in progressive neuromuscular disease and the role of stretching, orthotics, and surgery. Phys Med Rehabil Clin NAm 1998;9:187–211.
31. Farmer SE, James M. Contractures in orthopaedic and neurological conditions: a review of causes and treatment. Disabil Rehabil 2001; 23:549–558. [PubMed: 11451189]
32. Skalsky AJ, McDonald CM. Prevention and management of limb contractures in neuromuscular diseases. Phys Med Rehabil Clin N Am 2012;23:675–687. [PubMed: 22938881]
33. Sanoudou D, Haslett JN, Kho AT, et al. Expression profiling reveals altered satellite cell numbers and glycolytic enzyme transcription in nemaline myopathy muscle. Proc Natl Acad Sci U S A 2003;100: 4666–4671. [PubMed: 12677001]
34. Wei B, Jin JP. TNNT1, TNNT2, and TNNT3: isoform genes, regulation, and structure-function relationships. Gene 2016;582:1–13. [PubMed: 26774798]
35. Bodor GS, Survant L, Voss EM, et al. Cardiac troponin T composition in normal and regenerating human skeletal muscle. Clin Chem 1997; 43:476–484. [PubMed: 9068591]
36. Xu Z, Feng X, Dong J, et al. Cardiac troponin T and fast skeletal muscle denervation in ageing. J Cachexia Sarcopenia Muscle 2017; 8:808–823. [PubMed: 28419739]
37. Gangadharan B, Sunitha MS, Mukherjee S, et al. Molecular mechanisms and structural features of cardiomyopathy-causing troponin T mutants in the tropomyosin overlap region. Proc Natl Acad Sci U S A 2017;114:11115–11120. [PubMed: 28973951]
38. Liu B, Tikunova SB, Kline KP, et al. Disease-related cardiac troponins alter thin filament Ca2+ association and dissociation rates. PLoS One 2012;7:e38259. [PubMed: 22675533]
39. Oki K, Wei B, Feng HZ, Jin JP. The loss of slow skeletal muscle isoform of troponin T in spindle intrafusal fibres explains the pathophysiology of Amish nemaline myopathy. J Physiol 2019;597:3999–4012. [PubMed: 31148174]
40. Ogut O, Granzier H, Jin JP. Acidic and basic troponin T isoforms in mature fast-twitch skeletal muscle and effect on contractility. Am J Physiol 1999;276:C1162–C1170. [PubMed: 10329966]
41. Gomes AV, Guzman G, Zhao J, Potter JD. Cardiac troponin T isoforms affect the Ca2+ sensitivity and inhibition of force development. Insights into the role of troponin T isoforms in the heart. J Biol Chem 2002;277:35341–35349. [PubMed: 12093807]
42. Smith LL, Gupta VA, Beggs AH. Bridging integrator 1 (Bin1) deficiency in zebrafish results in centronuclear myopathy. Hum Mol Genet 2014;23:3566–3578. [PubMed: 24549043]
43. Gupta VA, Ravenscroft G, Shaheen R, et al. Identification of KLHL41 mutations implicates BTB-kelch-mediated ubiquitination as an alternate pathway to myofibrillar disruption in nemaline myopathy. Am J Hum Genet 2013;93:1108–1117. [PubMed: 24268659]
44. Dowling JJ, Vreede AP, Low SE, et al. Loss of myotubularin function results in T-tubule disorganization in zebrafish and human myo-tubular myopathy. PLoS Genet 2009;5:e1000372. [PubMed: 19197364]
45. Eisen JS, Smith JC. Controlling morpholino experiments: don’t stop making antisense. Development 2008;135:1735–1743. [PubMed: 18403413]
46. Stainier DYR, Raz E, Lawson ND, et al. Guidelines for morpholino use in zebrafish. PLoS Genet 2017;13:e1007000. [PubMed: 29049395]
47. Patel N, Smith LL, Faqeih E, et al. ZBTB42 mutation defines a novel lethal congenital contracture syndrome (LCCS6). Hum Mol Genet 2014;23:6584–6593. [PubMed: 25055871]
48. Ravenscroft G, Miyatake S, Lehtokari VL, et al. Mutations in KLHL40 are a frequent cause of severe autosomal-recessive nemaline myopathy. Am J Hum Genet 2013;93:6–18. [PubMed: 23746549]
49. Boyden SE, Mahoney LJ, Kawahara G, et al. Mutations in the satellite cell gene MEGF10 cause a recessive congenital myopathy with minicores. Neurogenetics 2012;13:115–124. [PubMed: 22371254]
50. Deniziak M, Thisse C, Rederstorff M, et al. Loss of selenoprotein N function causes disruption of muscle architecture in the zebrafish embryo. Exp Cell Res 2007;313:156–167. [PubMed: 17123513]

Author Manuscript Author Manuscript Author Manuscript Author Manuscript

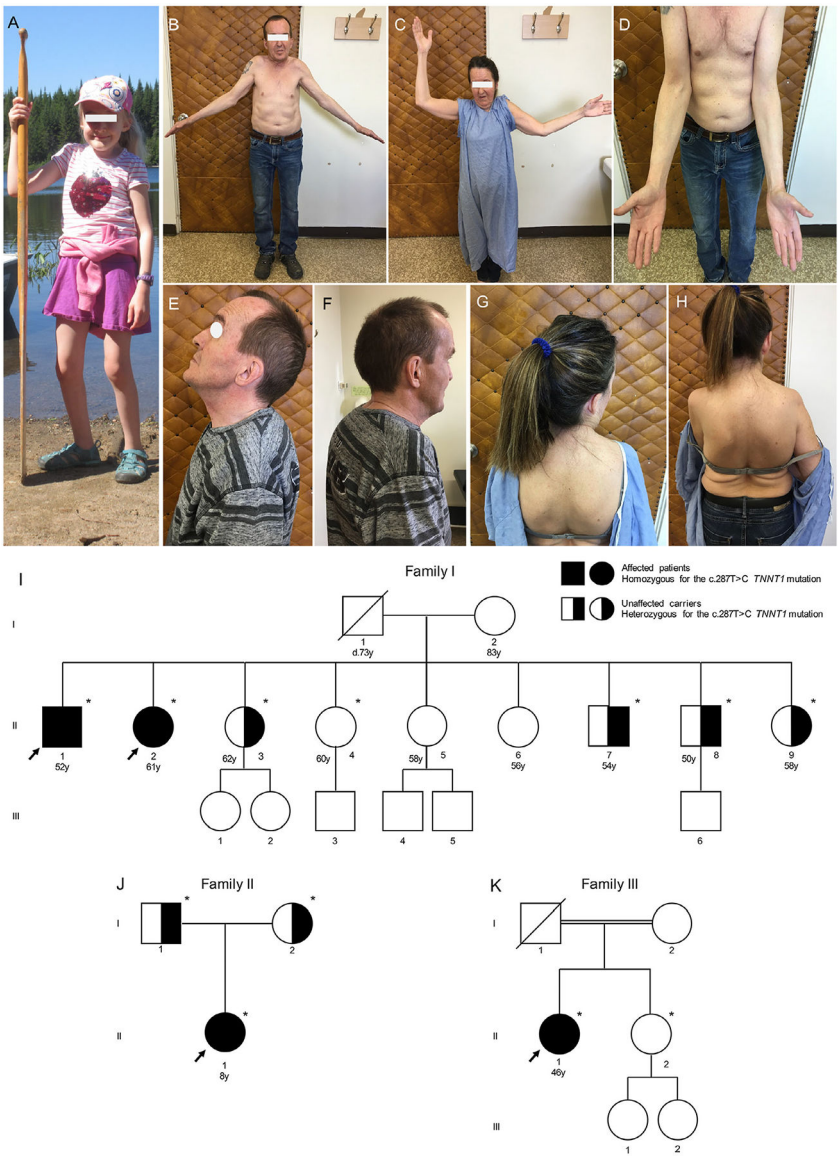

FIGURE 1:

Clinical findings and *TNNT1* variant segregation. (A) Patient III and (B–H) Patients I and II. (A) Flexion contractures of the hips and elbows, short stature, and decreased muscle bulk in Patient III. (B, C) Shoulder contractures significantly limiting abduction in Patients II (B) and I (C). (D) Elbow contractures in Patient II. (E, F) Rigid spine with limited cervical extension (E) and increased thoracic kyphosis (F) in Patient II. (G, H) Rigid spine with limited cervical range of motion (G) and kyphoscoliosis (H) in Patient I. (I–K) Family pedigrees of Family I (Patients I and II; I), Family II (Patient III; J), and Family III (Patient IV; K). Age at time of evaluation or at time of death is indicated. Arrows indicate the probands. Solid black shapes designate affected subjects homozygous for the c.287T>C (p.Leu96Pro) *TNNT1* gene variant. Half-solid black shapes designate unaffected (carrier for variant) subjects heterozygous for the c.287T>C (p.Leu96Pro) *TNNT1* gene variant. *Genetically tested individuals.

Author Manuscript Author Manuscript Author Manuscript Author Manuscript

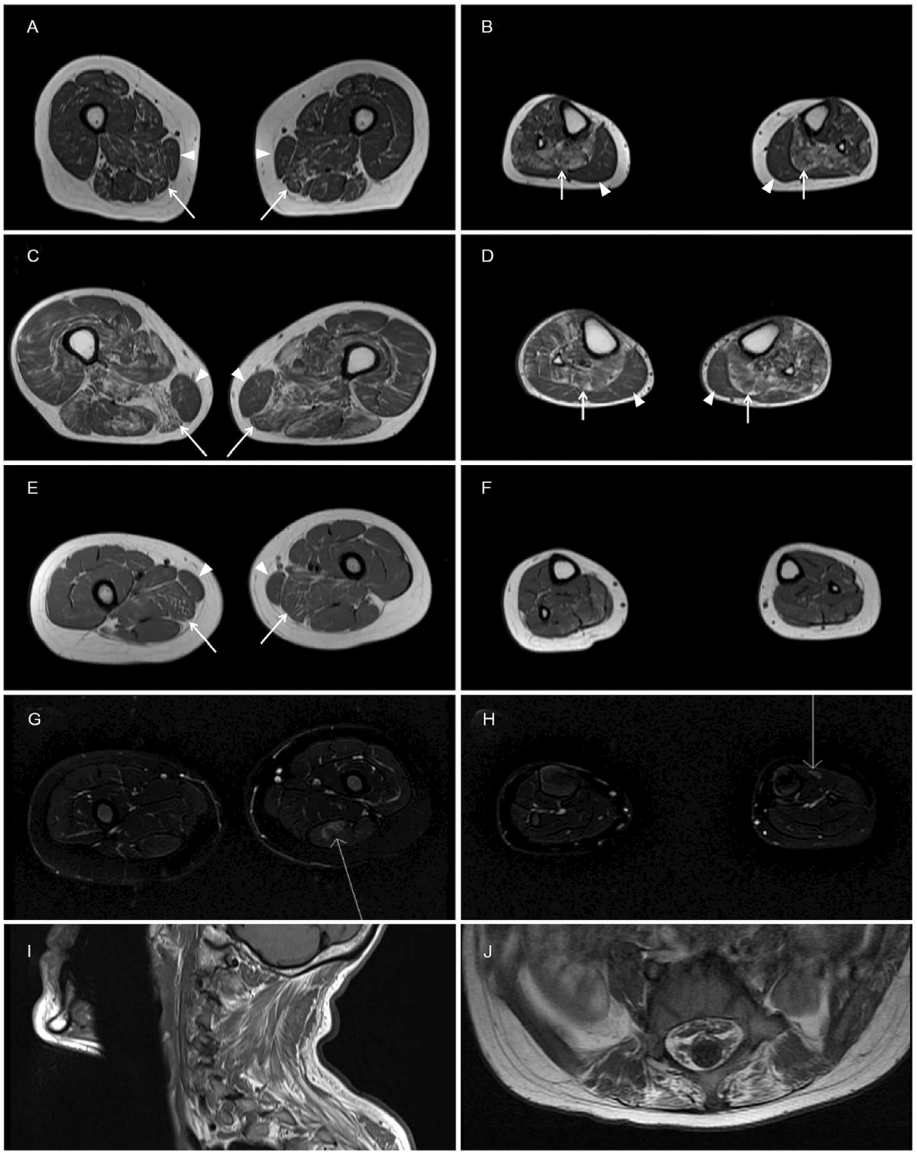

FIGURE 2:

Magnetic resonance imaging findings in the French Canadian *TNNT1* myopathy. (A–F) Axial T1-weighted images of thigh (A, C, E) and leg (B, D, F) muscles in Patient I at age 57 years (A, B), Patient II at age 53 years (C, D), and Patient III at age 6 years (E, F). (A, C, E) Atrophy and fibrofatty infiltration of the posterior thigh compartment mainly involving the semimembranosus *(arrows)* and adductor muscles, with relative sparing of the anterior compartment and gracilis muscle *(arrowheads)*. (B, D) Atrophy and fibrofatty infiltration predominating in the soleus *(arrows)* and the deep posterior leg compartment (tibialis posterior, flexor digitorum longus, and flexor hallucis longus), with sparing of the gastrocnemius muscles *(arrowheads)*. (F) Normal signal and morphology of distal leg muscles in Patient III. (G, H) Axial T2-weighted fat suppression images of thigh (G) and leg (H) muscles in Patient III at age 6 years obtained 1 week after an episode of rhabdomyolysis showing asymmetrical areas of hyperintensity suggestive of myoedema *(arrows)*. (I, J)

Author Manuscript Author Manuscript Author Manuscript Author Manuscript

Sagittal (I) and axial (J) T1-weighted images of paraspinal muscles in Patient II at age 50 years (I) and Patient III at age 6 years (J) showing diffuse atrophy and fibrofatty infiltration of the cervical (I) and lumbar paraspinal muscles (J).

Author Manuscript Author Manuscript Author Manuscript Author Manuscript

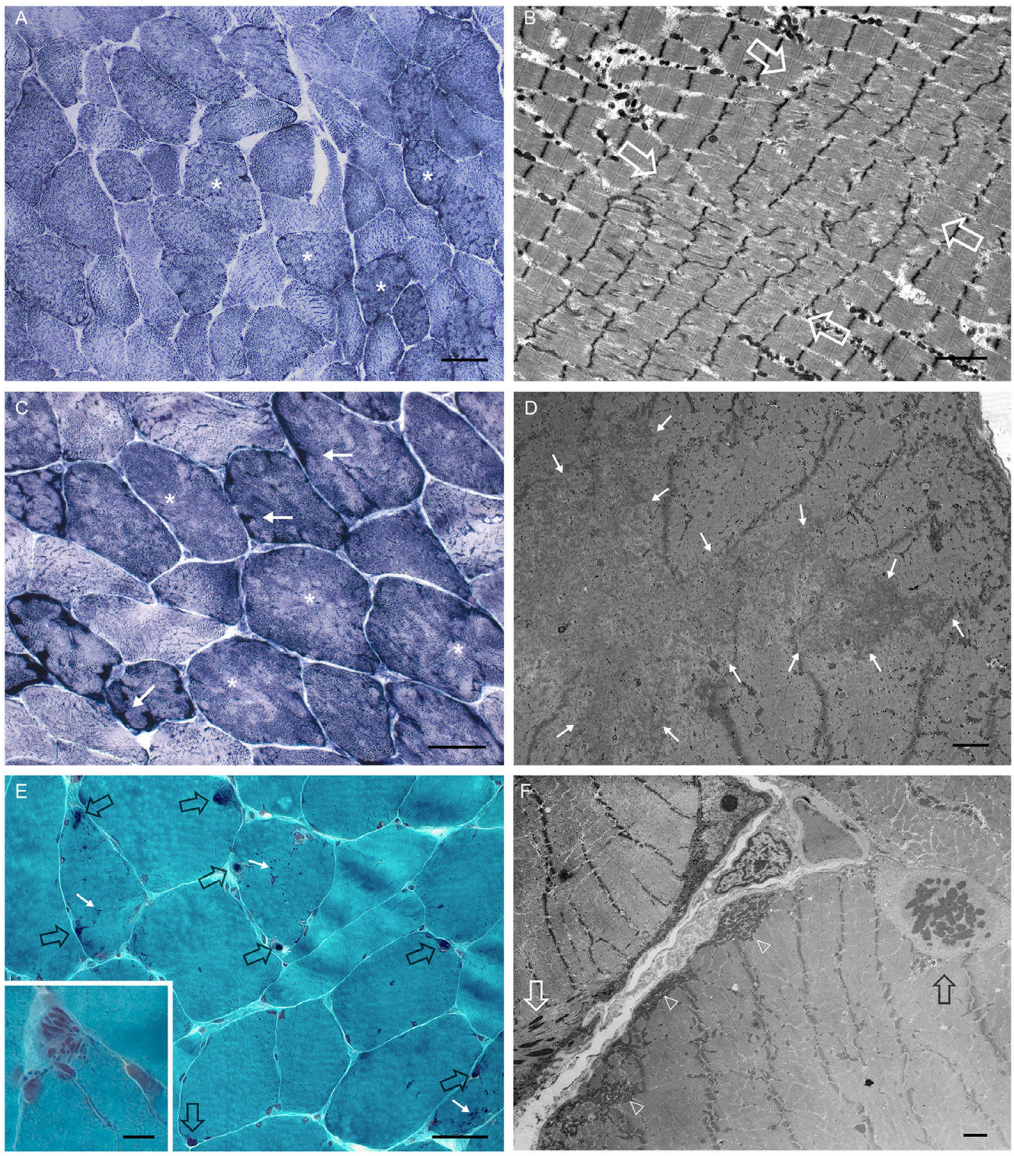

FIGURE 3:

Muscle pathology in the French Canadian *TNNT1* myopathy. Photomicrographs obtained from the biopsies of Patient III (A, B) and Patient I (C–F) illustrate the salient histologic features observed in this series. (A) Reduced nicotinamide adenine dinucleotide dehydrogenase-tetrazolium reductase (NADH-TR) preparation showing many fibers with small, irregular defects in staining consistent with multiminicores, some fibers *(asterisks)* also showing a slightly lobulated appearance due to localized subsarcolemmal accumulation of oxidative activity. (B) Electron micrograph showing in longitudinal orientation a focal area of myofibrillar disorganization with exclusion of mitochondria *(open arrows)*. (C) NADH-TR preparation showing coalescent minicores *(asterisks)* in most of the oxidative type fibers, many of them also showing marked lobular appearance *(arrows)*. (D) Electron photomicrograph in transverse orientation showing an irregular area of myofibrillar disorganization *(arrows)* corresponding to coalescent minicores. (E) Gomori trichrome

Author Manuscript Author Manuscript Author Manuscript Author Manuscript

showing many dark-staining type I fibers with subsarcolemmal inclusions *(open arrows)* composed of clusters of nemaline rods *(inset)*, and some with isolated intermyofibrillar rods *(white arrows)*. (F) Electron photomicrograph showing nemaline rods aligned with the sarcolemma *(open white arrow)*or in haphazard orientations forming a globular subsarcolemmal inclusion *(open black arrow)*; subsarcolemmal "pyramid" shaped accumulations of mitochondria *(open arrowheads)* imparting a lobular appearance to fibers on NADH-TR. Scale bars in A, C, E = 50μm; in B, D, F = 2μm; in inset = 10μm.

Author Manuscript Author Manuscript Author Manuscript Author Manuscript

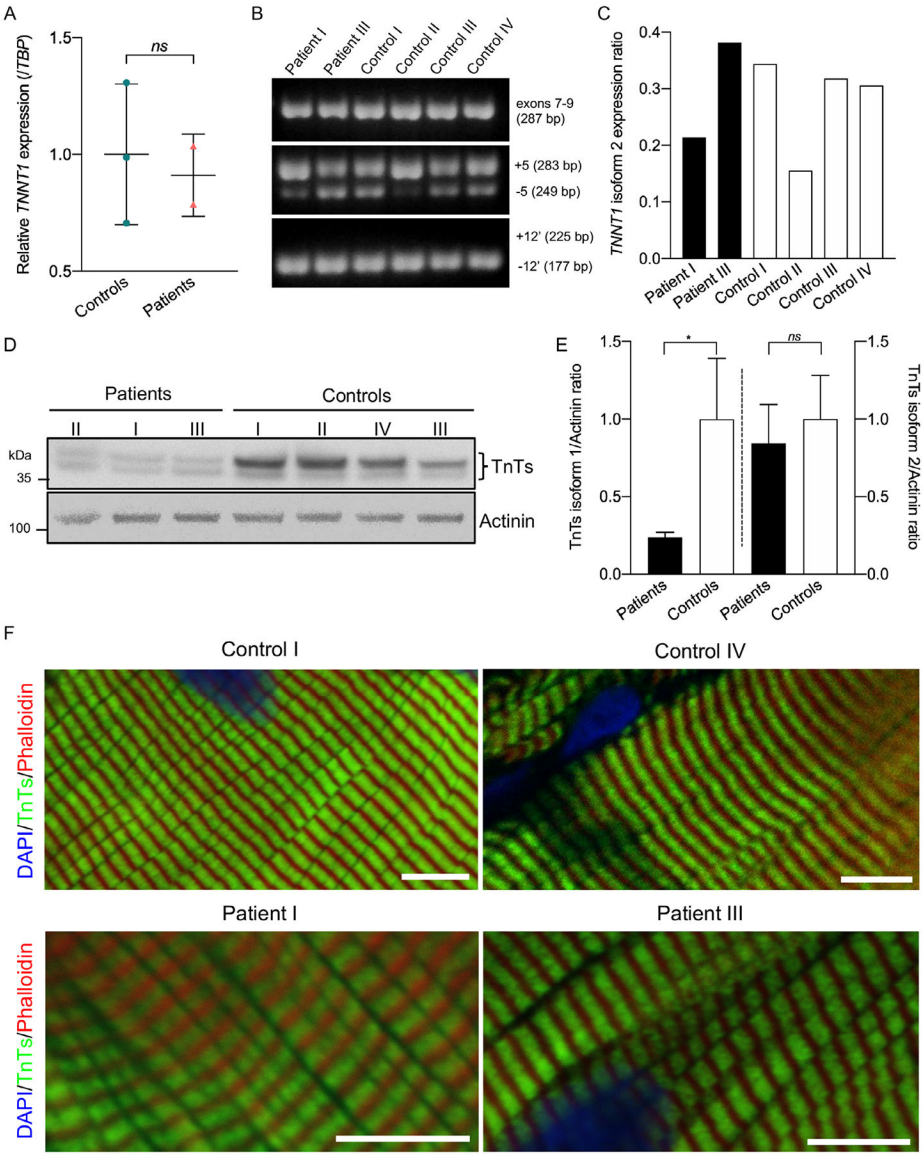

FIGURE 4:

Characterization of *TNNT1* gene expression, slow skeletal muscle troponin T (TnTs) protein levels, and subcellular localization. (A) Relative expression of *TNNT1* transcripts (NM_003283.6, NM_001126132.2, NM_001126133.2, NM_00129177.1) in controls (n = 3; Control I, Control II, Control IV) and patients (n = 2; Patient I, Patient III) normalized to TATA-box binding protein (*TBP*, NM_003194.3) mRNA levels as assessed by TaqMan probe-based reverse transcription (RT) quantitative polymerase chain reaction (PCR). For each gene assay, samples were run in duplicate. Values are represented as fold change of the mean value of control expression. Bars show mean ± standard deviation. ns = nonsignificant by 2-tailed Student t test. (B) RT-PCR analysis of *TNNT1* exon 7 to exon 9 amplicons (upper panel) and splicing of exon 5 (middle panel) and exon 12' (lower panel) in muscle biopsies of controls and patients. Samples from all 4 controls and Patients I and III were analyzed. Included (+5, +12') and excluded (−5, −12') exons along with the expected sizes

Author Manuscript Author Manuscript Author Manuscript Author Manuscript

(in base pairs) of the PCR products are indicated on the right of each panel. (C) Relative expression of *TNNT1* isoform 2 lacking exon 5 for individual controls and patients expressed as a ratio of the lower amplicon (−5) band intensity relative to the combined intensity of the 2 products (+5 and −5) on agarose gel. (D) Representative TnTs immunoblot of protein extracts from control and patient muscle biopsies. Bracket denotes TnTs isoforms 1 (high molecular weight splice form) and 2 (low molecular weight splice form lacking exon 5). Sarcomeric alpha-actinin was used as loading control. Samples from all 4 controls and Patients I, II, and III were analyzed. The experiment was repeated 3 times, and this blot is representative of the findings. (E) Expression ratios of TnTs isoforms 1 and 2 in control and patient muscle extracts. All ratios were normalized to sarcomeric alpha-actinin and expressed relative to controls. Bar graphs show mean ± standard deviation. $*p < 0.05$ by 2-tailed Student *t* test. (F) Representative single Z-slice confocal images of skeletal muscle from Controls I (deltoid) and IV (quadriceps) and Patients I (quadriceps) and III (quadriceps) immunolabeled for TnTs (Alexa Fluor 555, green), F-actin (Alexa Fluor 647-phalloidin, red), and nuclei (DAPI, blue). Analysis of raw confocal images by ImageJ using the thresholding method shows a decrease in TnTs fluorescent intensity of ~28% in patients as compared to controls. Scale bars = 5μm.

Author Manuscript Author Manuscript Author Manuscript Author Manuscript

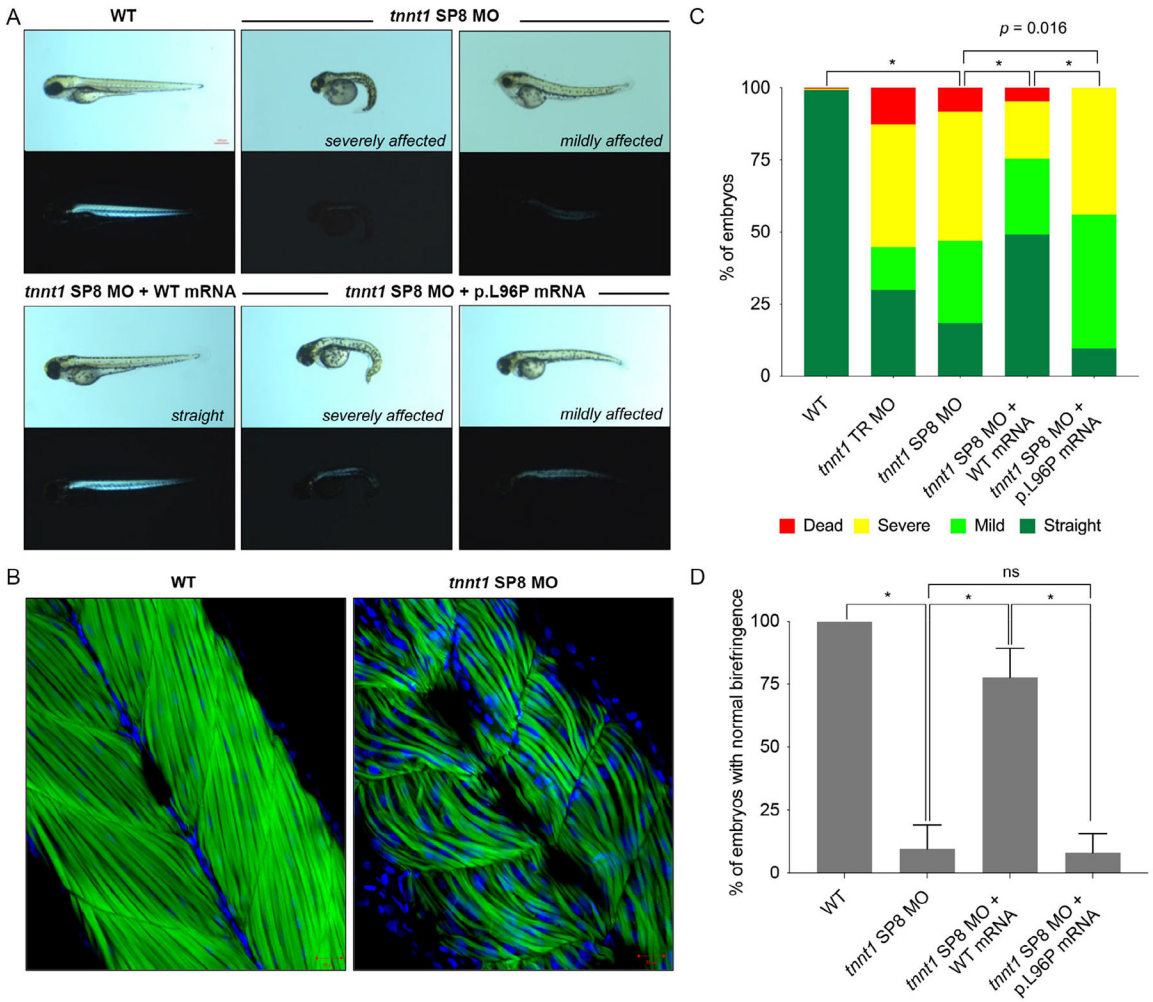

FIGURE 5:

Morpholino (MO)-based knockdown and rescue of zebrafish *tnnt1*. (A) Representative zebrafish (3 days postfertilization [dpf]) injected with *tnnt1* SP8-MO (top middle and right) display prominent truncal curvature and reduced birefringence under plane polarized light compared to wild-type (WT) larvae (top left). Overexpression of human WT *TNNT1* mRNA in *tnnt1* SP8-MO morphants restores the curvature and the birefringence (bottom left). In contrast, human *TNNT1* mRNA encoding the p.Leu96Pro mutation (p.L96P) fails to rescue the *tnnt1* SP8-MO morphant phenotype (bottom middle and right). Matched pairs of images illustrate appearance under light microscopy above the same field showing birefringence under plane polarized light. (B) Actin (green) and nuclear (blue) stains of 3-dpf *tnnt1* SP8-MO morphants show decreased numbers and disorganization of muscle fibers (right) compared to WT larvae (left). (C) Microinjection of either *tnnt1* TR-MO or *tnnt1* SP8-MO morpholinos leads to significant reduction in numbers of morphologically normal “straight” embryos. Coinjection of human WT *TNNT1* mRNA in SP8-MO morphants significantly increases the number of straight embryos. In contrast, overexpression of mRNA with the p.Leu96Pro mutation with *tnnt1* SP8-MO fails to rescue the truncal curvature. (D) Similarly, reduced birefringence in the *tnnt1* SP8-MO morphants is restored upon overexpressing the

Author Manuscript Author Manuscript Author Manuscript Author Manuscript

human WT mRNA, whereas mRNA with the p.Leu96Pro mutation fails to rescue the birefringence. For each experimental condition, between 130 and 232 embryos from 3 to 8 different clutches were scored. Error bars in D reflect standard deviation between clutches. Numbers for uninjected WT controls were pooled across experiments, totaling 605 embryos from 20 clutches. $*p < 0.00001$ for each indicated comparison for numbers of “straight” (C) or normally birefringent (D) embryos; ns indicates $p > 0.05$.

Author Manuscript Author Manuscript Author Manuscript Author Manuscript

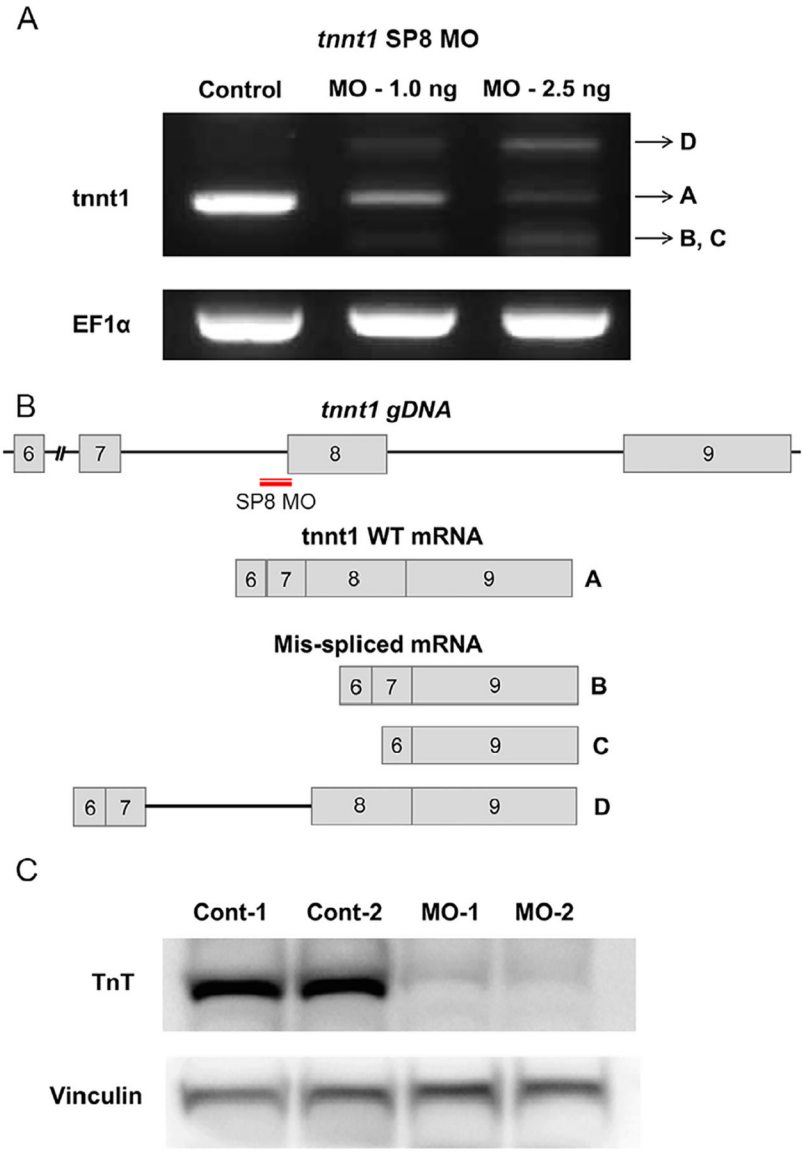

FIGURE 6:

Morpholino (MO) knockdown of *tnnt1* results in mRNA missplicing and decreased protein levels. (A) Reverse transcription polymerase chain reaction shows a single band of *tnnt1* transcript (labeled A) in uninjected control zebrafish. With increased doses of morpholino injections, the intensity of the wild-type (WT) *tnnt1* transcript diminishes, and additional products representing misspliced mRNA are observed. (B) WT *tnnt1* genomic DNA (gDNA) is transcribed into *tnnt1* mRNA as shown. The SP8-MO results in 3 different misspliced forms of *tnnt1* as represented by transcripts B–D. (C) Western blots of MO knockdowns (n = 40) show decreased levels of slow skeletal muscle troponin T protein expression in *tnnt1* morphants compared to uninjected control (cont) zebrafish.

Author Manuscript Author Manuscript Author Manuscript Author Manuscript

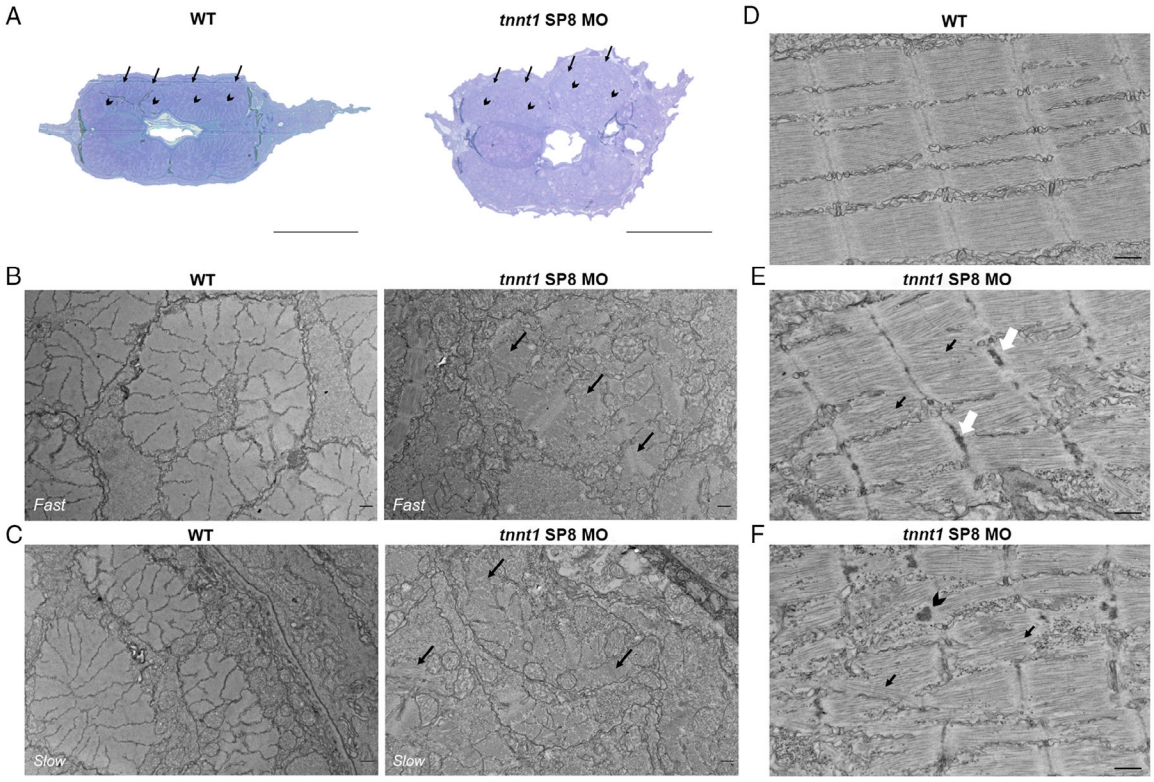

FIGURE 7:

Electron microscopy of *tnnt1* zebrafish morphants. (A) Cross sections of *tnnt1* morphants stained with toluidine blue reveal muscle disorganization in both fast *(arrowheads)* and slow *(arrows)* muscles as well as the presence of centrally located cores. (B, C) Electron microscopy of 3 days postfertilization (dpf) *tnnt1* zebrafish morphant cross sections reveal that both fast (B) and slow (C) muscle have areas of disorganized muscle structure *(black arrows)*, with myofibrils running in different planes compared to the highly organized structure of the wild-type (WT) larvae. (D) Electron microscopy of longitudinal cross sections of WT larvae at 3 dpf. (E) Electron microscopy of 3-dpf *tnnt1* morphants reveals areas of muscle disorganization *(black arrows)* and increased thickness of Z-lines *(white arrows)* compared with the wild-type larvae. (F) Protein aggregation *(arrowhead)* is observed in 3 dpf *tnnt1* morphants along with areas of sarcomeric disorganization *(black arrows)*. Scale bars in A = 10μm; in B–F =500nm.

Author Manuscript Author Manuscript Author Manuscript Author Manuscript

Table.

Clinical and Pathological Features of Patients with the French Canadian *TNNT1* Myopathy

Characteristic	Patient I, Family I	Patient II, Family I	Patient III, Family II	Patient IV, Family III
Gender	F	M	F	F
Age of recognition	Infancy	Infancy	Birth	Infancy
Age at latest examination, yr	62	53	8	46
Initial symptoms	Gross motor milestones delay, proximal muscle weakness	Gross motor milestones delay, proximal muscle weakness	Congenital scoliosis, arthrogryposis multiplex congenita, congenital hip luxation	Gross motor milestones delay, proximal muscle weakness, scoliosis, congenital hip luxation
Ambulatory status	Walking unaided, unable to climb stairs without support or to run	Walking unaided, unable to climb stairs without support or to run	Walking long distance unaided, able to jump and climb a few stairs	Wheelchair at age 14 yr, walking 20 steps with aid, unable to run or climb stairs
Clinical features	Limb-girdle weakness (MRC = 4/5), kyphoscoliosis, few episodes of rhabdomyolysis	Limb-girdle weakness (MRC = 3–4/5), Gowers sign, kyphoscoliosis, recurrent episodes of rhabdomyolysis	Limb-girdle weakness (MRC = 4/5), Gowers sign, scoliosis, recurrent episodes of rhabdomyolysis	Muscle weakness (MRC = 4/5) of neck flexors, hip girdle, and tibialis anterior, scoliosis, a few episodes of rhabdomyolysis
Spinal rigidity and contractures	Rigid spine and contractures: shoulders, elbows, wrists, fingers, hips, ankles	Rigid spine and contractures: shoulders, elbows, wrists, fingers, hips, ankles	Rigid spine and contractures: hips and elbows	Rigid spine and contractures: hips and ankles
CK (normal = 50–200U/l)	900–1,000U/l	250–300U/l	350–700U/l	200–673U/l
Peak CK during rhabdomyolysis	30,000U/l	50,000U/l	5,200U/l	22,000U/l
Respiratory involvement	Mild restrictive syndrome (FVC = 83%, FEV_1 = 86%)	Moderate restrictive syndrome (FVC = 62%, FEV_1 = 58%), severe OSA requiring BiPAP	Severe restrictive syndrome (FVC = 38%, FEV_1 = 37%), moderate OSA requiring BiPAP	Severe restrictive syndrome (FVC = 19%) requiring BiPAP throughout day and night
Muscle pathology	Multiminicores and nemaline rods in type I fibers, lobulated fibers, mild fatty infiltration, moderate variability in fiber size and shape	Multiminicores and nemaline rods in type I fibers, lobulated fibers, mild fatty infiltration, selective type II fiber atrophy, moderate variability in fiber size and shape	Deltoid (age 5 yr): multiminicores in type I fibers, lobulated fibers. Quadriceps (age 8 yr): same as in deltoid, and mild fibrosis, fatty infiltration, and scattered regenerative fibers	Multiminicores in type I fibers, mild fibrosis, moderate variability in fiber size and shape

BiPAP = bilevel positive airway pressure noninvasive ventilation; CK = creatine kinase; F = female; FEV_1 = forced expiratory volume in 1 second; FVC = forced vital capacity; M = male; MRC = Medical Research Council scale for muscle strength; OSA = obstructive sleep apnea.

Ann Neurol. Author manuscript; available in PMC 2021 April 01.